



OPEN ACCESS

EDITED BY

Rita Silva-Gomes,
University of Minho, Portugal

REVIEWED BY

Roland Lang,
University Hospital Erlangen, German
Giovanni Delogu,
University of Parma, Italy
Henrique Machado,
University of Minho, Portugal

*CORRESPONDENCE

Margarida Saraiva
✉ margarida.saraiva@i3s.up.pt

†These authors share first authorship

‡PRESENT ADDRESS

Ana Raquel Maceiras,
Lymphocyte Regulation, GIMM - Gulbenkian
Institute for Molecular Medicine, Lisbon,
Portugal

RECEIVED 14 October 2025

REVISED 19 November 2025

ACCEPTED 20 November 2025

PUBLISHED 16 December 2025

CITATION

Maceiras AR, Silva ML, Couto J, Gonçalves R, Silva M, Macedo S, Machado D, Indafa I, Sifna A, Malaca CD, Namara NI, Sanca L, Rodrigues PNS, Viveiros M, Rudolf F, Wejse C, Cá B and Saraiva M (2025) Activation of nuclear receptors correlates with tuberculosis severity and is a target for host-directed therapy.
Front. Cell. Infect. Microbiol. 15:1724798.
doi: 10.3389/fcimb.2025.1724798

COPYRIGHT

© 2025 Maceiras, Silva, Couto, Gonçalves, Silva, Macedo, Machado, Indafa, Sifna, Malaca, Namara, Sanca, Rodrigues, Viveiros, Rudolf, Wejse, Cá and Saraiva. This is an open-access article distributed under the terms of the [Creative Commons Attribution License \(CC BY\)](https://creativecommons.org/licenses/by/4.0/). The use, distribution or reproduction in other forums is permitted, provided the original author(s) and the copyright owner(s) are credited and that the original publication in this journal is cited, in accordance with accepted academic practice. No use, distribution or reproduction is permitted which does not comply with these terms.

Activation of nuclear receptors correlates with tuberculosis severity and is a target for host-directed therapy

Ana Raquel Maceiras^{1,2,3††}, Marta L. Silva^{1,4†}, Joana Couto¹, Rute Gonçalves^{1,4}, Marco Silva^{1,4}, Salvador Macedo¹, Diana Machado⁵, Iaiá Indafa^{6,7}, Armando Sifna^{6,7}, Cesaltina D. Malaca^{6,7}, Nelson I. Namara^{6,7}, Lilica Sanca^{6,7}, Pedro N. S. Rodrigues^{1,2}, Miguel Viveiros⁵, Frauke Rudolf^{7,8}, Christian Wejse^{7,9}, Baltazar Cá^{1,2,6,7} and Margarida Saraiva^{1,2*}

¹I3S - Instituto de Investigação e Inovação em Saúde, University of Porto, Porto, Portugal,

²BMC - Instituto de Biologia Molecular e Celular, University of Porto, Porto, Portugal, ³Wellcome Sanger Institute, Cambridge, United Kingdom, ⁴Doctoral Program in Molecular and Cell Biology, ICBAS - Instituto de Ciências Biomédicas Abel Salazar, University of Porto, Porto, Portugal, ⁵Global Health and Tropical Medicine, Associate Laboratory in Translation and Innovation Towards Global Health, Instituto de Higiene e Medicina Tropical, Universidade Nova de Lisboa, Lisbon, Portugal, ⁶INASA - Instituto Nacional de Saúde Pública da Guiné-Bissau, Bissau, Guinea-Bissau, ⁷Bandim Health Project, InDepth Network, Bissau, Guinea-Bissau, ⁸Department of Infectious Diseases, Aarhus University Hospital, Aarhus, Denmark, ⁹GloHAU Center for Global Health, Aarhus University, Aarhus, Denmark

Introduction: The immune response to *Mycobacterium tuberculosis* is accompanied by metabolic adaptations that fuel host immunity, but that are exploited by the pathogen to ensure persistence and growth. Activation of nuclear receptors, such as liver-X-receptors (LXR), orchestrate macrophage immunometabolic adaptations to infection and globally associate with tuberculosis (TB) protection.

Methods: We interrogated available transcriptomic datasets of whole blood from TB patients or *M. tuberculosis* aerosol-infected mice to assess the expression of the signal by nuclear receptors (SNR) and LXR pathways and its correlation with disease severity. In vitro (macrophages) and in vivo (mouse model) *M. tuberculosis* infections were used for functional validation of the LXR act as a potential host-directed therapy.

Results: We show that both the SNR and the LXR pathways are detected in the whole blood of TB patients and that their expression correlates with disease severity. Accordingly, the activation of the LXR pathway progressively increases in the lungs of *M. tuberculosis*-infected C57BL/6 and C3HeB/FeJ mice. Pharmacologic activation of LXR, specifically at the chronic stage of infection, improved infection outcomes and significantly prolonged the survival of the highly susceptible C3HeB/FeJ mice. Common to both mouse models and to in vitro macrophage infections, LXR activation enhanced bacterial control together with an increase in extracellular cholesterol levels.

Discussion: We propose that progressive LXR activation is required to fine-tune host cholesterol availability during *M. tuberculosis* infections and restrict access to this nutrient during chronic stages of infections. Collectively, we identify the SNR/LXR pathways as potential biomarkers of TB severity and timely LXR activation as a candidate host-directed therapy.

KEYWORDS

tuberculosis, *Mycobacterium tuberculosis*, nuclear receptor (NR), host-directed therapies, transcriptomics

Introduction

Tuberculosis (TB) remains a leading cause of death worldwide. In 2023, an estimated 10.4 million people fell ill with TB and 1.25 million died of this disease (Organization, W.H, 2024). The outcomes of infection by *Mycobacterium tuberculosis* vary from elimination, to latency, to incipient, subclinical or active disease of different severities (Coussens et al., 2024). These different outcomes are largely determined by the host immune response (O'Garra et al., 2013; Scriba et al., 2024). The study of the whole blood transcriptome of TB patients revealed a neutrophil-driven type I interferon (IFN)-dependent signature (Berry et al., 2010), and has provided important cues on host protective versus detrimental pathways (Singhania et al., 2018a). This whole blood signature is recapitulated in *M. tuberculosis* HN878-infected C3HeB/FeJ mice (Moreira-Teixeira et al., 2020a), where type I IFN blockade or neutrophil depletion resulted in disease improvement (Moreira-Teixeira et al., 2020b). Thus, pathways discovered in human disease and tested in tractable mouse models hold great potential to advance our understanding of TB pathogenesis.

Macrophages are central to TB pathogenesis, serving as host cells for *M. tuberculosis*, initiating the immune response and adapting to the infection through a series of immunometabolic changes (Russell et al., 2025) (Kumar et al., 2019). *In vitro*, in response to live *M. tuberculosis* infection, macrophages shift their metabolism towards glycolysis (Gleeson et al., 2016; Lachmandas et al., 2016; Mendonca et al., 2022; Fernandes et al., 2025), and display a prominent metabolic signature of cholesterol metabolism (Chandra et al., 2022). The lungs of *M. tuberculosis*-infected mice also change their energetic metabolic profile (Shi et al., 2015), with alveolar macrophages being characterized by a strong ox-phos signature, and interstitial monocytes by a glycolytic shift (Huang et al., 2018; Pisu et al., 2020; Pisu et al., 2021). A realignment of the host lipid metabolism also occurs in the granuloma, with a high abundance of cholesterol, cholesteryl esters, triacylglycerols and lactosylceramide identified in the human caseum (Kim et al., 2010). This realignment is explored by *M. tuberculosis*, which requires cholesterol for survival during infection (Pandey and Sassetti, 2008; Soto-Ramirez et al., 2017). Data from the mouse model of infection show that the cholesterol catabolic pathway of *M. tuberculosis* is

implicated in TB pathogenesis, mostly during the chronic phase of infection (Pandey and Sassetti, 2008; Chang et al., 2009; Yam et al., 2009; Nesbitt et al., 2010; Wilburn et al., 2018) and a transcriptional signature of cholesterol catabolism was found in *M. tuberculosis* isolated from sputum samples of TB patients (Garton et al., 2008; Lai et al., 2021). Cholestenone, a mycobacterial-derived oxidized derivative of cholesterol, was also detected in the sputum of TB patients, highlighting its potential interest as a novel biomarker in TB (Chandra et al., 2022). In line with the key role of cholesterol during TB, small chemical compounds capable of inhibiting cholesterol utilization by *M. tuberculosis* have been identified as promising therapeutic tools (VanderVen et al., 2015; Wilburn et al., 2022; Brown et al., 2023). In particular, perturbing cAMP signaling in the mouse model of *M. tuberculosis* infection impacts disease pathology, bacterial physiology and host responses (Kathayat and VanderVen, 2024). Targeting the host cholesterol metabolism also showed promising results in experimental *M. tuberculosis* infection. Administration of all trans-retinoic acid (ATRA), which induces cholesterol efflux in macrophages (Wheelwright et al., 2014) or of cholesterol-lowering drugs (statins) (Parihar et al., 2014; Dutta et al., 2020) reduced the bacterial burdens in infected mice.

The nuclear receptor family members, liver-X-receptors (LXR), are key regulators of both intracellular cholesterol homeostasis and inflammation (Leopold Wager et al., 2019a; Glaria et al., 2020), playing a role in protection to several intracellular bacteria (Joseph et al., 2004; Valledor et al., 2004; Matalonga et al., 2017), including *M. tuberculosis* (Leopold Wager et al., 2019b). Single nucleotide polymorphisms in LXR genes associated with genetic susceptibility to TB in the Chinese Han population (Han et al., 2014). Activation of the LXR in cultures of *M. tuberculosis*-infected THP1 cells decreased lipid body formation and improved bacterial control (Bouttier et al., 2016; Ahsan et al., 2018). In contrast, silencing LXR α in THP1 cells led to increased bacterial burdens (Mahajan et al., 2012). In the mouse model of *M. tuberculosis* intra-tracheal infection, LXR deficiency associated with poorer outcomes of disease, whilst their activation improved bacterial control (Korf et al., 2009). Given the high homology between human and mouse LXR α and LXR β , the high expression of LXR α in myeloid cells and the promising findings in the context of infectious diseases and TB, we sought to investigate whether the activation of nuclear receptors

is detected in TB patients and whether their *in vivo* modulation in mouse models that recapitulate the human whole blood transcriptional signature of TB (Moreira-Teixeira et al., 2020a) may impact disease outcomes.

Here, we show that the ‘signaling by nuclear receptors’ (SNR) pathway (Sever and Glass, 2013) is detected in the whole blood of TB patients across independent TB datasets, and accompanied TB severity. Focusing in the LXR component of the nuclear receptor superfamily, we show its dynamic activation in the lungs of both C57BL/6 and C3HeB/FeJ mice upon aerosol infection with *M. tuberculosis* HN878. Importantly, pharmacologic modulation of LXR improved outcomes of infection in both mouse models, being time-dependent, maximal upon LXR activation in the chronic stage of infection, and connected to cholesterol efflux, without major alterations to the immune response. In all, by combining whole blood transcriptomics of TB patients and experimental mouse data, we reveal a candidate molecular marker of TB severity and demonstrate the potential of timely reinforcing protective pathways, such as LXR-mediated cholesterol efflux, to improve TB outcomes.

Results

The signaling by nuclear receptors pathway is activated during TB and correlates with disease severity

To investigate whether the activation of the SNR pathway may be detected in the whole blood of TB patients, we performed gene set enrichment analysis (GSEA) in two previously published RNAseq datasets. The London dataset (referred to as Berry - London) comprises healthy donors, individuals with latent TB and those with active TB, and the South Africa dataset (referred to as Berry - South Africa) includes participants with latent or active TB (Berry et al., 2010; Singhania et al., 2018b). The SNR pathway was detected in both datasets, in position 101/227 for the Berry London dataset, and in position 112/246 in the case of the South Africa dataset, upon ranking by adjusted p-value (Supplementary Tables 1, 2). Of the 315 genes forming the SNR reactome pathway “R-HSA-9006931; signal by nuclear receptors” a total of 25 genes were found to be differentially expressed in at least one of the tested cohorts, being notoriously higher in TB patients as compared with healthy donors or latently infected individuals (Figure 1A). Since a certain degree of heterogeneity in the expression of the SNR genes was detected at the patient level, we questioned whether this heterogeneous expression might reflect TB disease severity. Using the Berry - London dataset, we analyzed how the eigengene expression of the SNR varied according to the extent of radiologic disease based on prior chest x-ray stratification (Berry et al., 2010). This analysis was not possible for the South Africa dataset, due to absence of clinical data. Increased expression of the SNR pathway indeed accompanied disease severity, presenting a positive and significant Spearman correlation ($\rho=0.62$, $p=0.002$; Figure 1B).

Increased expression of the LXR pathway in humans and mice upon *M. tuberculosis* infection

Among the various SNR family members, we next decided to focus our study on the LXR pathway, a member of the nuclear receptor superfamily previously associated with intracellular cholesterol homeostasis and inflammation (Leopold Wager et al., 2019a; Glaria et al., 2020) and TB protection (Korf et al., 2009; Han et al., 2014; Bouttief et al., 2016; Ahsan et al., 2018), two observations that may be linked. As above we interrogated the two whole blood transcriptome datasets, this time for genes that code proteins downstream the LXR receptors involved in cholesterol regulation or inflammatory responses. As for the SNR pathway, the expression of the selected genes of the LXR pathway was heterogeneous and higher in TB patients than in controls (Figure 1C). Furthermore, we also found a significant positive Spearman correlation ($\rho=0.60$, $p=0.004$) between the LXR pathway eigengene expression and disease severity (Figure 1D).

We also analyzed the activation of the LXR pathway in C57BL/6 and C3HeB/FeJ mice infected via aerosol with *M. tuberculosis* isolate HN878, using previously generated RNAseq datasets for these models at the peak of disease (Moreira-Teixeira et al., 2020a). We found that the LXR pathway was highly represented both in blood (Figure 2A) and lung (Figure 2B) of infected mice, regardless of the mouse genetic background. To investigate the kinetics of expression of the LXR pathway at the site of infection, we measured the mRNA transcripts of several genes downstream of LXR activation in the lungs of either mouse strain before infection (day 0) or at days 6, 12 and 25 post-infection. These time points were chosen based on the dynamics of bacterial load accumulation in the lungs of *M. tuberculosis* HN878-infected C57BL/6 or C3HeB/FeJ mice (Supplementary Figure 1A). With the exception of the *ApoE* gene in C57BL/6 mice, whose expression was not altered with infection, the other tested genes were generally upregulated over-time upon infection in both mouse strains (Figure 2C). These data further support the link between the activation of nuclear receptors and TB disease progression. However, some differences were detected for the expression profile of some genes in C3HeB/FeJ mice between the RNAseq data (Figure 2A, B) and the lung qPCR (Figure 2C), which might be related to differences in the initial infection dose, which was high for the RNAseq experiments and low for the qPCR ones.

The beneficial effect of LXR activation during *M. tuberculosis* aerosol infection of C57BL/6 mice is time-dependent

LXR $\alpha\beta$ double-deficient mice were shown to be more susceptible to intra-tracheal *M. tuberculosis* infection, displaying higher CFUs and lung histopathology, whereas activating the LXR pathway prior or post-infection demonstrated improved lung bacterial burdens, possibly due to increased early neutrophil

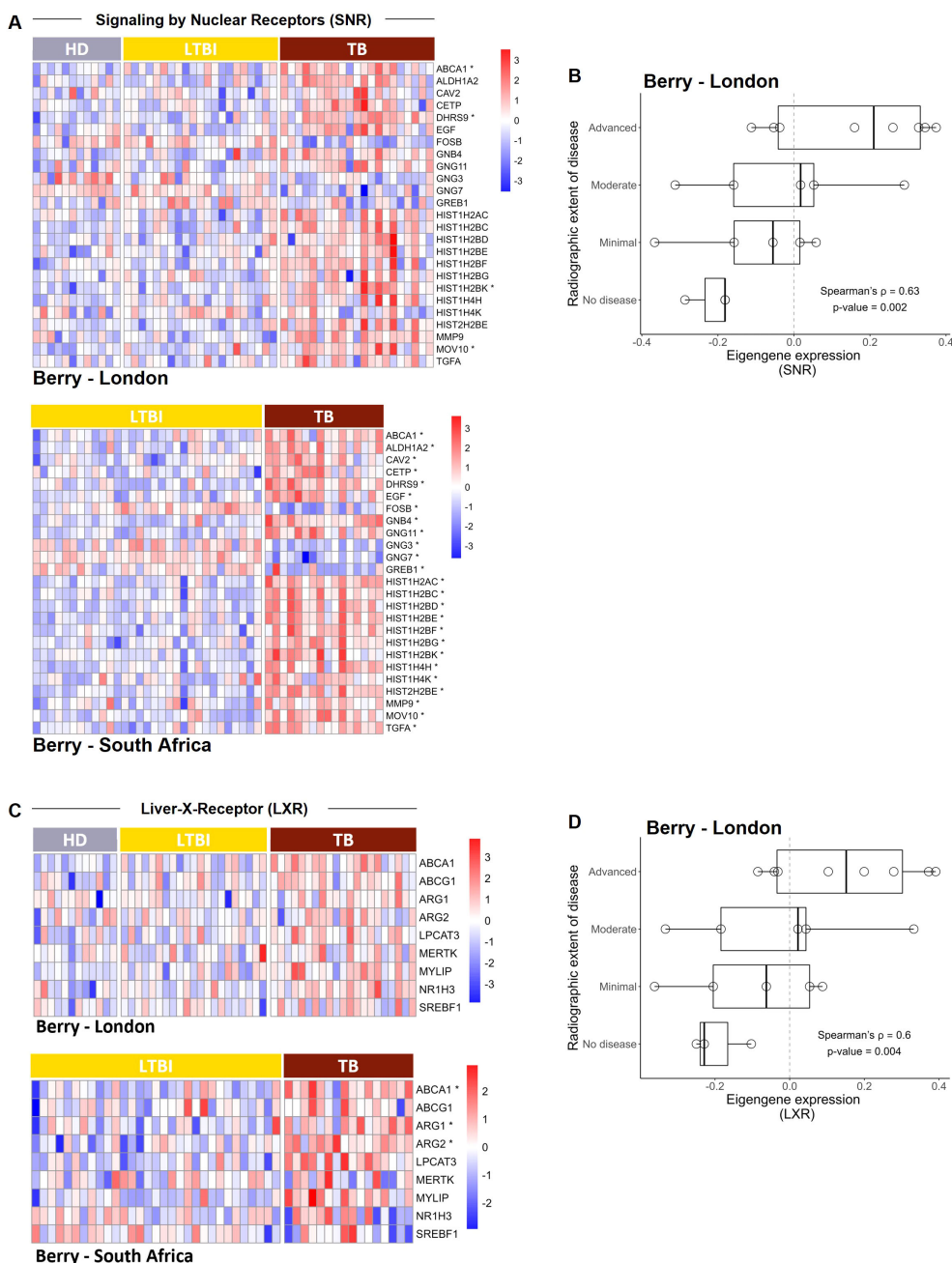


FIGURE 1

The signaling by nuclear receptors and liver-X-receptor pathways are detected in the blood of TB patients and correlate with TB severity. (A) Heatmaps showing the relative expression of genes detected from the SNR pathway for the Berry-London and the Berry-South Africa cohorts for healthy donors (HD), latent TB infection (LTBI) and TB patients (TB). (B) Box and whisker plot showing the distribution of the eigengene expression of the SNR across the radiographic extent of disease, classifying the TB patients from the Berry-London cohort. (C) Heatmaps showing the relative expression of genes detected from the LXR pathway for healthy donors (HD), latent TB infection (LTBI) and TB patients (TB) from the Berry-London and Berry-South Africa datasets. (D) Box and whisker plot showing the distribution of the eigengene expression of the LXR across the radiographic extent of disease, classifying the TB patients from the Berry-London cohort. In (A, C), each column represents an individual; differentially expressed genes for the specific cohort are identified with an *. In (B, D), each point represents one individual and the correlation between the two variables was determined by Spearman correlation analysis, with the ρ and p values indicated.

recruitment and enhanced CD4 T cell responses (Korf et al., 2009). However, the pharmacologic activation of this pathway during aerosol infection of mouse models that better recapitulate the human whole blood TB signature had not been tested. Furthermore, considering our findings showing a dynamic

transcription of the LXR pathway during *M. tuberculosis* infection, we hypothesized that the timing of LXR potentiation might impact the final result. To investigate these hypotheses, we administered the LXR agonist T0901317 to C57BL/6 mice 7 days prior to infection, or day 6, 12 or 18 post- *M. tuberculosis* HN878

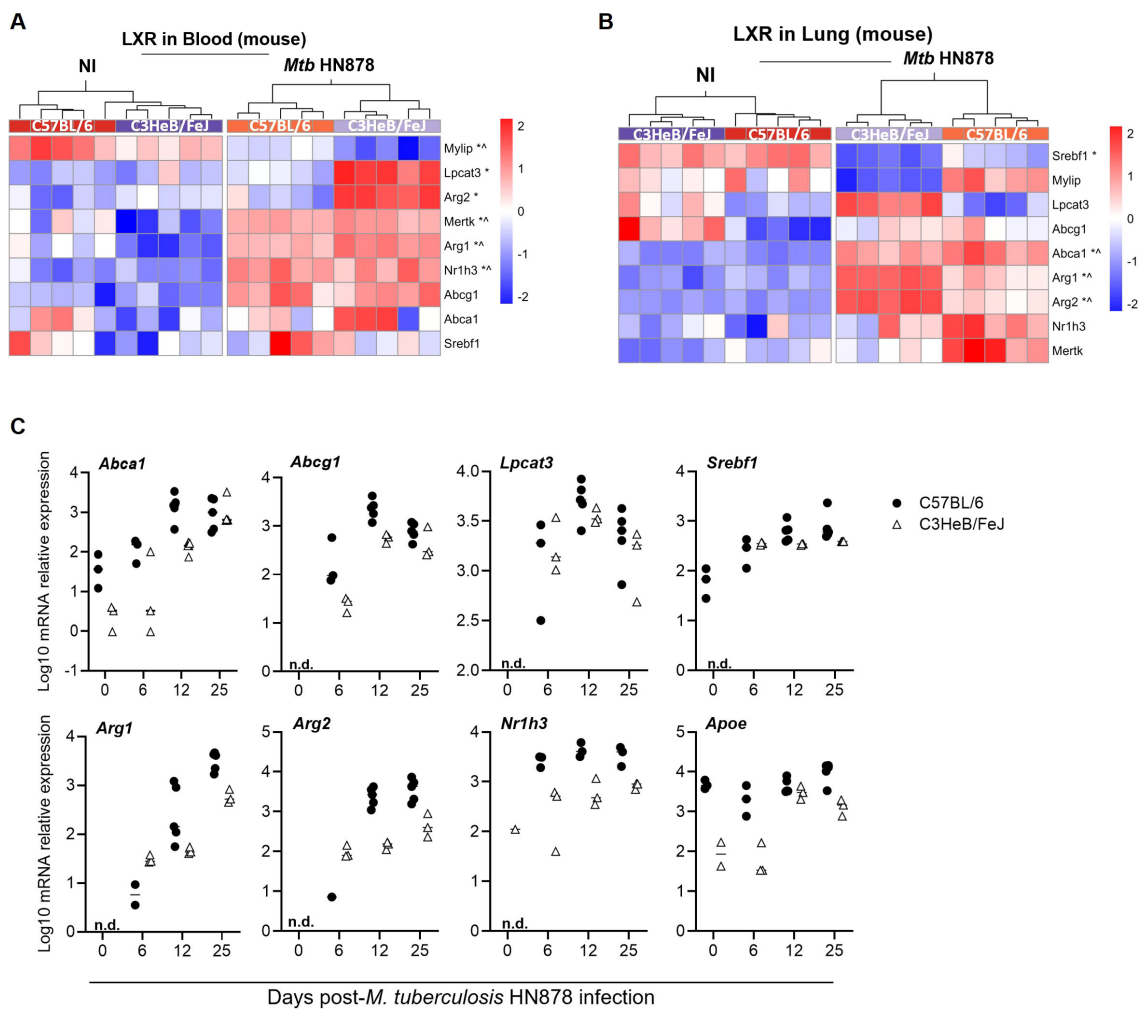


FIGURE 2

Liver-X-receptor activation in experimental (mouse) TB. (A, B) Heatmaps showing the relative expression of selected genes from the LXR pathway in the blood (A) and lung (B) of non-infected (NI) or aerosol-infected C3HeB/FeJ or C57BL/6 mice. Data are from infections with high doses of *M. tuberculosis* HN878, from a publicly available RNAseq dataset. For both heatmaps, each column represents an individual mouse, normalized gene expression by gene (Z-score by row) is presented and differentially expressed genes are identified with an *, for C3HeB/FeJ mice or ^, for C57BL/6 mice. (C) Transcriptional analysis of the indicated genes of the LXR pathway by qPCR in the lungs of C57BL/6 (circles) or C3HeB/FeJ (triangles) mice aerosol-infected with *M. tuberculosis* isolate HN878 (580 and 209 CFU delivered to the lung of C57BL/6 or C3HeB/FeJ mice respectively), prior to (day 0) or at different time-points (day 6–12–25) post-infection. Each dot represents an individual mouse in one experiment. n.d., not detected.

aerosol infection. Prophylactic administration of the LXR agonist or its administration on days 6 or 12 post-infection did not impact the weight loss curve of vehicle or LXR-activated infected mice (Figure 3A, top panels). In contrast, mice that received the LXR agonist from day 18 post-infection did not lose as much weight as the vehicle group (Figure 3A, top panels), suggesting a time-dependent beneficial effect of the administered regimen. On day 24/25 post-infection, at which point the control (vehicle) group reached the peak of disease, we analyzed the lung bacterial burdens for all groups. Prophylactic administration of the LXR agonist resulted in a minimal decrease of lung bacterial burdens (Figure 3A, bottom panel). Early activation of the LXR pathway (day 6 post-infection) did not impact lung bacterial burdens, whereas activation from day 12 post-infection resulted in a modest decrease in lung bacterial burdens (Figure 3A, bottom

panel). Strikingly, a pronounced decrease of over a log₁₀ in bacterial numbers in the lungs of treated mice was observed upon activation of the LXR pathway from day 18 post-infection (Figure 3A, bottom panel).

Focusing on the effect of LXR administration at this time-point, we investigated whether the observed protection might be due to restriction of bacterial growth. The increase in the lung bacterial burden from day 18 to the end-point of the experiment (day 25) was much larger in control mice than in those that received the LXR agonist (respectively, 47.9 versus 5.58 increase; Figure 3B). Despite this improved control of bacterial growth, the % of lesioned lung area (Figure 3C) was not significantly altered in LXR-treated mice and the lung lesion inflammatory score showed only a modest decrease (Figure 3D; Supplementary Figure 1B). In an apparent paradox with its increased expression as the infection progresses,

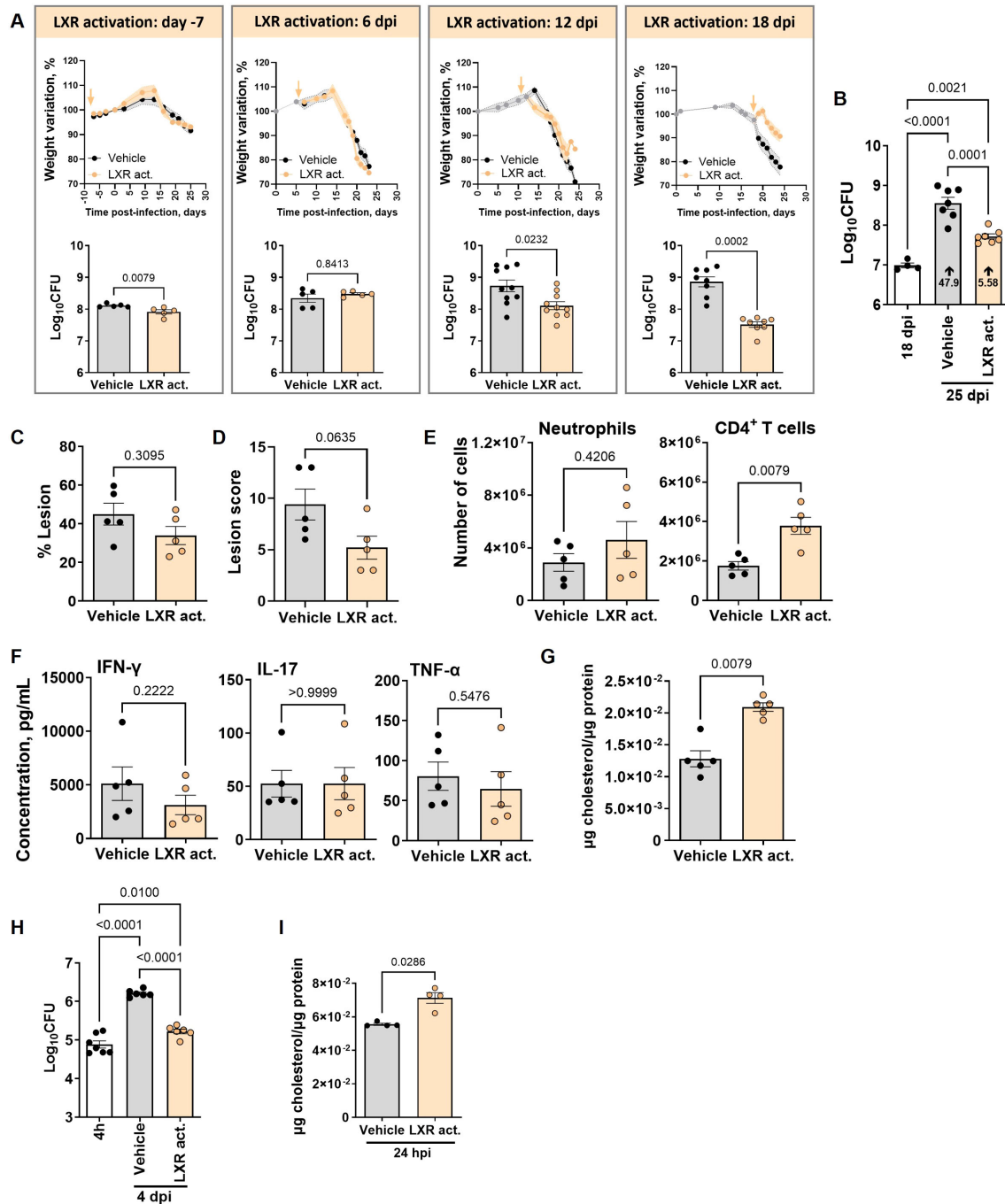


FIGURE 3

Time-dependent effect of liver-X-receptor activation in controlling *M. tuberculosis* infection of C57BL/6 mice. C57BL/6 mice were treated with the LXR activator T0901317 at days 7 prior to infection (-7), or days 6, 12 or 18 post-aerosol infection with *M. tuberculosis* isolate HN878 (with infections ranging from 503 to 853 CFU delivered to the lung). (A) Body weight variation for control (vehicle; grey) or treated (orange) mice during the course of the experiment (top panels) and bacterial burdens in CFU determined on day 25 post-infection (bottom panels). The arrows in the top panels represent the initial time-point of LXR agonist administration. (B) C57BL/6 were infected as above and bacterial loads determined on days 18 (prior to vehicle or LXR administration) and 25 (experimental end-point) post-infection. The fold increase in lung bacterial burden from day 18 to day 25 in each experimental group is represented in the respective bars. (C) For the mice infected in (A) and treated with the LXR activator from day 18 post-infection, the % of lung lesioned area (C), lesion score (D), number of neutrophils and CD4⁺ T cells in the lung (E), levels of the indicated cytokines (F) and total cholesterol (G) in the lung supernatants were determined on day 25 post-infection for control (vehicle; grey bars) or treated (orange bars) mice. Each dot represents the mean of five animals with SEM shaded (A, top panels) or independent mice [mean \pm SEM; (A), bottom panels, (B-G)]. Activation of the LXR pathway at -7 or +6 days was tested once, and on days 12 or 18 in two independent experiments. (H, I) Bone marrow-derived macrophages (BMDM) from C57BL/6 mice were infected with *M. tuberculosis* HN878 (MOI=2) and 4 h later treated or not with 100 nM of the LXR activator. Bacterial loads (H) were determined 4 h and 4 days post-infection and total cholesterol detected in the supernatants of the infected cultures 24 h post-infection (I). Data are mean \pm SEM, with each dot representing one individual well. Mann-Whitney U tests were used to identify statistical differences between the two groups. p-values are indicated and considered significant if ≤ 0.05 . dpi, days post infection; hpi, hour post-infection; Mtb, *M. tuberculosis*.

these data suggest that reinforcing the LXR pathway near the peak of infection improved bacterial control with no major effect on tissue damage restriction.

To further investigate this apparent paradox, we next analyzed the immune cell populations present in the lungs of vehicle or LXR-treated mice (Supplementary Figure 1C). An overall increase of the various immune cell populations was detected in LXR-treated mice (Supplementary Figure 1D). Of particular interest in determining pathology versus protection in TB are neutrophils versus CD4 T cells (Moreira-Teixeira et al., 2020a). Notably, *M. tuberculosis*-infected mice that received the LXR agonist on day 18 post-infection showed similar numbers of neutrophils and increased numbers of CD4 T cells (Figure 3E), as compared to control mice. The general increase in lung immune cells, together with a similar presence of neutrophils, in LXR-treated mice may explain the fact that the lung infiltrated area and histological score remain similar to that of control mice, despite improved control of bacterial growth. Because the increase in the numbers of CD4 T cells was not accompanied by an increase of effector cytokines namely IFN- γ , IL-17 or TNF in the lung supernatants (Figure 3F), nor by a different organization of lung lesions in the lungs of LXR-treated animals (Figures 3C, D), we hypothesized that the protective effect of LXR activation may be linked to other mechanisms.

LXR activation enhances the macrophage bacterial control and the extracellular levels of cholesterol

Given the relevance of the LXR pathway to cholesterol metabolism (Luo et al., 2020) and of cholesterol to *M. tuberculosis* pathogenesis (Roth et al., 2024), we hypothesized that pharmacological activation of the LXR may enhance cholesterol efflux from host cells depriving *M. tuberculosis* of this carbon source. This would be in line with the enhanced expression of cholesterol transporters induced by the LXR agonist T0901317 in *M. tuberculosis*-infected THP1 cells (Bouttier et al., 2016). Indeed, we detected increased levels of cholesterol in the supernatants of lungs of *M. tuberculosis* HN878 infected C57BL/6 mice treated with the agonist from day 18 to day 25 post-infection (Figure 3G). To investigate if this effect of LXR activation on the host was time-dependent, we activated the LXR pathway between days 6 and 12. LXR activation during this period did not impact the levels of extracellular cholesterol (Supplementary Figure 2A). Also, at the end of the LXR activation, only a minor effect was observed in bacterial burdens (Supplementary Figure 2B), which was not sustained over time, as by day 25 post-infection no differences in the lung CFUs were observed between the two groups (Supplementary Figure 2C).

Since previous studies demonstrated that LXR activation in THP1 cells limited *M. tuberculosis* growth (Bouttier et al., 2016; Ahsan et al., 2018), we next infected mouse bone marrow-derived macrophages (BMDM) with *M. tuberculosis* HN878 and allowed the infection to progress for 4 days in the absence (vehicle) or presence of the LXR activator. Activation of the LXR pathway

decreased intracellular bacterial growth as compared to vehicle controls (Figure 3H), while increasing the levels of extracellular cholesterol (Figure 3I). This protective effect of the LXR activator in BMDM was not exclusive to infection with *M. tuberculosis* HN878, as similar results were obtained upon infection of macrophages with a clinical isolate from lineage 4 (Supplementary Figure 2D). Comparable findings were observed in THP1 cells (Supplementary Figure 2E). In line with our *in vivo* data, increased bacterial control was invariably accompanied by increased extracellular cholesterol amounts (Supplementary Figure 2D, E). Since activation of the LXR pathway in macrophages reduced *Salmonella enterica* serovar Typhimurium phagocytosis (Matalonga et al., 2017), we tested if a similar mechanism would operate in *M. tuberculosis*. However, no differences in bacterial burdens were detected in the presence of the LXR agonist during the first 4 h of infection (Supplementary Figure 2F). Furthermore, the presence of the LXR activator in axenic media did not directly impact the growth of *M. tuberculosis* even when cholesterol was provided as an energy source (Supplementary Figure 2G), which supports a host-mediated effect of the LXR activator.

Impact of LXR activation in *M. tuberculosis* infections of C3HeB/FeJ mice

Having demonstrated a protective effect of late LXR activation in C57BL/6 mice, we tested the same intervention in C3HeB/FeJ mice, which better recapitulate the immune and histological features of human TB (Moreira-Teixeira et al., 2020a; Moreira-Teixeira et al., 2020b). Treatment of C3HeB/FeJ mice with the LXR activator at 18 days post-aerosol infection with *M. tuberculosis* HN878 led to a decrease in lung bacterial burdens (Figure 4A) and an increase in the levels of extracellular cholesterol (Figure 4B). The differences seen between vehicle and LXR-activated C3HeB/FeJ infected mice recapitulated those detected for C57BL/6 ones, but were less pronounced. In contrast with the general increase in immune cells observed in the case of LXR-treated C57BL/6 mice (Supplementary Figure 1D), activation of LXR in infected C3HeB/FeJ mice did not change most of the lung immune cell populations (Supplementary Figure 3A). However, also in sharp contrast with what was observed in C57BL/6 mice, it resulted in a significant increase in the number of lung neutrophils and a significant decrease in CD4 T cells (Supplementary Figure 3A).

An increase in neutrophils and decrease in CD4 T cells has been associated with TB susceptibility in different studies (Moreira-Teixeira et al., 2020a; Branchett et al., 2025; Gern et al., 2025). Thus, we questioned whether prolonging the LXR activation in infected C3HeB/FeJ mice would indeed improve disease outcomes or only transiently enhance bacterial control. To test this, the administration of the LXR activator was prolonged up to day 50 post-infection. Whereas the vehicle-treated animals showed pronounced weight loss (Supplementary Figure 3B), reaching humane end-points before day 40 post-infection, those receiving the LXR activator survived significantly longer, with 6/12 animals

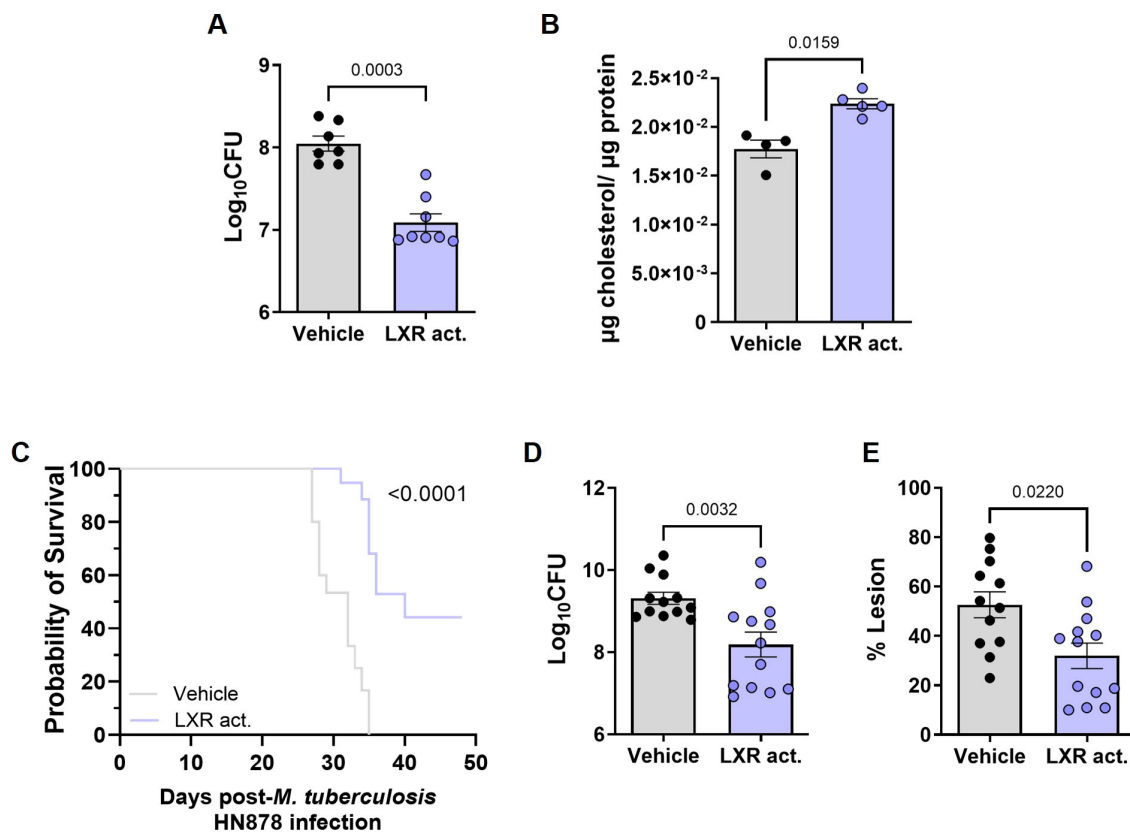


FIGURE 4

LXR activation reduces lung bacterial burdens and prolongs survival of *M. tuberculosis*-infected C3HeB/FeJ mice. C3HeB/FeJ mice were aerosol-infected with *M. tuberculosis* isolate HN878 (203 or 271 CFU delivered to the lung) and administered with the LXR activator T0901317 or vehicle control from day 18 post-infection. On day 24 post-infection, the lung bacterial burdens (A) and total cholesterol in the lung homogenates (B) were quantified. (C) Survival curve (humane end-points defined based on over 20% weight loss or severely compromised respiratory function) for C3HeB/FeJ animals infected with *M. tuberculosis* as above and treated with vehicle or the LXR agonist for up to 50 days. Lung bacterial burdens (D) and percentage of lung lesioned area (E) for each animal enrolling the survival curve at its respective end-point. (A, B, D, E) Vehicle and treated groups are represented by grey or blue bars, respectively. Data are mean ± SEM. Each dot represents an individual mouse. (C, D, E) Data is pooled from 2 independent experiments (dose of infection 203 and 271). Mann-Whitney U tests were used to identify statistical differences between the two groups. p-values are indicated and considered significant if ≤ 0.05 . In (C) A Log-rank (Mantel-Cox) test was used to compare the survival curves; p-values are indicated and considered significant if ≤ 0.05 .

still performing well at the end-point (Figure 4C; Supplementary Figure 3B). Of note, when pooling all animals irrespective of their time-of-death, the LXR-treated C3HeB/FeJ mice showed lower bacterial burdens and lesioned area than vehicle controls (Figure 4D, E). Therefore, LXR administration also improved the outcome of infection in C3HeB/FeJ mice, significantly prolonging their survival.

Discussion

TB remains a high-burden disease, with important challenges being the development of improved diagnosis methods and better, less toxic and shorter treatment regimens (Dartois et al., 2025). The study of the whole blood transcriptome of TB patients has allowed the identification of immune signatures of disease, together with their phenotypic heterogeneity, evolution during infection and resolution upon treatment (Berry et al., 2010; Singhania et al., 2018b; Tabone et al., 2021). Moreover, it has shed important light

into the mechanisms of TB pathogenesis advancing the discovery of potential targets for host-directed therapies (Singhania et al., 2018a; Moreira-Teixeira et al., 2020b). Here, we resorted to available transcriptomic datasets of TB patients and *M. tuberculosis*-infected mice to investigate the expression of nuclear receptors during TB. Nuclear receptors are a superfamily of transcriptional regulators linking lipid metabolism, inflammation and the immune system (Sever and Glass, 2013), with a relatively well established role in TB (Leopold Wager et al., 2019b). We show that the overall SNR pathway was enriched in TB patients from London and South Africa, as compared to the respective healthy controls. Moreover, for the London dataset, we found that the extent of SNR activation in the blood increased with the radiologic extent of disease. Thus, our study provides initial evidence of the SNR pathway as a molecular candidate of TB disease progression and, potentially, TB severity. Even though our findings are validated in different sets of patients, the small numbers included represent a limitation of the study. Future validation of the SNR as a relevant marker in TB is important, as stratifying TB patients is increasingly acknowledged

as a key step to devise rational strategies to treat TB, namely to adjust the required duration of current regimens in a patient-centered way (Dartois et al., 2025).

We further focused our study on the LXR pathway, a specific molecular component of the SNR, because LXRs are expressed in macrophages, the preferred cellular niche for *M. tuberculosis*, and their activation regulates the metabolism of cholesterol, an important nutrient for this pathogen across different phases of infection, from phagocytosis to chronicity (Chen et al., 2024). Furthermore, previous studies highlight the protective effect of LXRs during *in vitro* (Mahajan et al., 2012; Bouttier et al., 2016; Ahsan et al., 2018) and *in vivo* (Korf et al., 2009) *M. tuberculosis* infections. We detected the activation of selected genes of the LXR pathway in the blood of TB patients across the aforementioned datasets, and reported a positive correlation between the LXR eigengene and the extent of radiologic disease, further hinting at the relevance of this pathway in TB. Moreover, we investigated the dynamics, effects and underlying mechanisms of the LXR activation in mouse models that reflect key features of the human disease: aerosol route of infection with an isolate of *M. tuberculosis* that allows for a whole blood transcriptomic signature recapitulating that seen in TB patients (Moreira-Teixeira et al., 2020a). Our study thus departs from a previous one using intra-tracheal infection with *M. tuberculosis* H37Rv laboratory reference strain (Korf et al., 2009), confirming some findings, but also revealing new ones. We report a progressive increase of the expression of several genes downstream the LXR pathway in the lungs of *M. tuberculosis* HN878- aerosol infected C57BL/6 and C3HeB/FeJ mice, and also detected their expression at the peak of disease in the lungs and blood of these mice. This enhanced lung expression of the LXR pathway as the infection progresses is in line with our human data and with a previous study, which tested a smaller set of LXR responsive genes in the bronchoalveolar lavage cells of mice infected intra-tracheally with *M. tuberculosis* H37Rv strain (Korf et al., 2009). It will be important in future studies to characterize the activation of the LXR pathway during infection beyond gene expression, as well as to identify which molecular cues trigger it.

Collectively, our analyses of the SNR/LXR expression in human TB and mouse models support a link between the activation of these pathways and disease progression. In the context of the established protective role of LXR in TB (Korf et al., 2009; Mahajan et al., 2012; Han et al., 2014; Bouttier et al., 2016; Ahsan et al., 2018), these findings may seem counterintuitive: how would a pathway whose expression increases with disease severity be protective? Further adding to this apparent paradox, in our experimental models, reinforcing the LXR pathway prior to or early on post-infection did not result in enhanced protection. The lack of effect of prophylactic LXR activation contrasts previous results (Korf et al., 2009), possibly due to the difference in the route of administration (aerosol versus intra-tracheal) and the strain of *M. tuberculosis* used (HN878 versus H37Rv). Interestingly, reinforcing the LXR pathway at the peak of its natural activation markedly improved *M. tuberculosis* growth control by the two mouse strains. In particular, this intervention significantly prolonged the survival of the highly susceptible C3HeB/FeJ mice. Thus, the LXR activation

by the host is likely to both reflect the progression of infection and represent a mechanism to restrict *M. tuberculosis* growth triggered during chronic stages of infection. The molecular cues activating and regulating LXR activation remain unknown, but it is possible that the accumulation of oxysterols in the lungs of infected mice play a role (Ngo et al., 2022). This accumulation may result from metabolic alterations in the host cells, notably macrophages, but also be promoted by the pathogen, as *M. tuberculosis* encodes several enzymes capable of hydroxylating cholesterol and generating LXR agonists (Capyk et al., 2009; Ouellet et al., 2010; Wilburn et al., 2018; Varaksa et al., 2021). Oxysterols are gaining importance as immune modulators in bacterial and viral infections (Foo et al., 2022) and are therefore of interest to further study in the context of TB.

We hypothesized that the mechanism underlying the time-dependent beneficial effect of LXR activation might be linked to alterations to intracellular cholesterol availability, a key nutrient for *M. tuberculosis* specifically during the chronic stage of infection (Pandey and Sasseti, 2008; Chang et al., 2009; Yam et al., 2009; Hu et al., 2010; Nesbitt et al., 2010). Increased activity of LXR has been previously associated to cholesterol export. Although we cannot exclude that a simultaneously increase of intracellular cholesterol may occur, an increase in the extracellular levels of cholesterol was indeed detected *in vivo* in the lungs of both C57BL/6 and C3HeB/FeJ mice that benefited from receiving the LXR agonist upon infection. Moreover, a similar increase was detected *in vitro* in BMDM cultures infected with *M. tuberculosis* HN878, or with an isolate of *M. tuberculosis* belonging to lineage 4. This is relevant, because strain specific differences in the ability to metabolize lipids, specifically cholesterol have been reported (Mooapanar et al., 2023). Although it is impossible to capture the full breath of host-*M. tuberculosis* interactions, our findings suggest cholesterol efflux and subsequent nutrient deprivation as the common axis linking the pharmacological activation of LXR with *M. tuberculosis* growth restriction. The mechanisms downstream LXR activation and leading to increased cholesterol efflux remain unknown, being important to address in future studies. These mechanisms possibly include the upregulation of cholesterol exporters in specific immune cells. Of note, the LXR-mediated protection may however be disrupted in the context of TB and metabolic comorbidities, such as diabetes (Ngo et al., 2022). Also of note, other cholesterol targeting strategies have been tested during *M. tuberculosis* infection (Parihar et al., 2014; Wheelwright et al., 2014; Dutta et al., 2020), but none reduced the bacterial burdens in infected mice to the extent we report here. This higher success of the LXR activation may be due to different modes of action, as well as experimental design, namely the time of activation which we show to be an important variable.

Interestingly, our *in vivo* data suggest that a remodeling of the immune response induced by LXR activation may not be a determinant factor underlying protection. In *M. tuberculosis*-infected C57BL/6 mice, administration of the LXR agonist contributed to an overall increase of immune cells in the lungs, the only exception being neutrophils. This global increase of immune cells may explain the fact that the lung infiltrated area

remained similar to that of control mice. The increase of CD4 T cells is in line with a previous report of LXR activation during intra-tracheal *M. tuberculosis* infection (Korf et al., 2009). However, unlike that study, we saw no evidence of increased Th1/Th17 cell responses, as the amounts of IFN- γ and IL-17 proteins present in the lung supernatants were comparable in control or LXR-treated mice. In C3HeB/FeJ infected mice, the activation of the LXR pathway resulted in decreased CD4 T cell and increased neutrophils being recruited to the lung. This divergence of protective versus detrimental immune responses in C57BL/6 versus C3HeB/FeJ mice, did not compromise the ultimately similar outcome of *M. tuberculosis* control. Thus, we propose a model where in addition to any possible adjustments to the immune response caused by LXR activation, nutrient limitation may act as the main mechanism for the beneficial action of LXR potentiation in tractable mouse models of TB.

Taken together, our findings suggest that progressive LXR activation may be required to fine-tune macrophage responses and cholesterol availability during *M. tuberculosis* infections. During initial stages of infection low LXR activation might be required to limit its anti-inflammatory function (Glaria et al., 2020) and ensure that cholesterol is available for key macrophage functions (Chen et al., 2024). Potent activation of the LXR during initial stages might lead to premature increase of Arg1, a molecule shown to limit host control of *M. tuberculosis* (El Kasmi et al., 2008). Later on, activation of LXR likely restricts the pathogen's access to cholesterol, which is a key nutrient for *M. tuberculosis* during chronic stages of infections. It is important to mention that at different host-pathogen interfaces, pharmacological modulation of the LXR pathway may yield similar host-protective results through distinct complex regulatory actions. For example, LXR activation is also protective during *S. Typhimurium* infections, but in that case involve CD38/NAD/cytoskeleton rearrangements which impact the phagocytic process (Matalonga et al., 2017).

In summary, our study expands the growing field of host metabolic regulation during infection, by proposing the SNR pathway as a possible biomarker of TB severity and cholesterol modulation by timely LXR activation as a host-directed therapy of interest in TB. Rational stratification of TB patients may impact the design of better therapeutic strategies, while improving LXR agonists for clinical use in TB, as well as testing their effects at even later time-points post-infection (once the lung lesions show the typical consolidated structure) alone or as adjuvants to TB antibiotherapy, are exciting avenues of research. Finally, our study contributes to two broader concepts in TB: that not all pathways reflecting disease severity might be detrimental, and that reinforcing protective pathways from a therapeutic perspective may require timely interventions.

Methods

Study approval

Animal experiments followed the ARRIVE guidelines, the 2010/63/EU Directive and were approved by the i3S Animal Ethics

Committee and the Portuguese National Authority for Animal Health (DGAV; #018413/2021-11-24).

Sex as a biological variable

Our study examined male and female mice, and similar results were found for both sexes.

RNAseq data analyses

Mouse whole-blood and lung RNAseq data from (Moreira-Teixeira et al., 2020a) were downloaded from SRA (GEO accession code GSE140945). The quality of raw sequencing data and the presence of adaptors were initially assessed using FastQC. Low-quality reads with less than 36 nucleotides long, adapters, leading bases with quality below 3, and trailing bases when the average quality per base was below 15 for regions of 4 bases were removed using Trimmomatic v0.39 (Bolger et al., 2014). HISAT2 v2.2.1 was then used to align the remaining reads to the *Mus musculus* genome Ensembl GRCm38 (release 84) followed by the usage of StringTie v2.1.6 to obtain gene-level counts (Pertea et al., 2015; Kim et al., 2019). The obtained counting table as well as whole-blood RNAseq count matrices from the Berry London and Berry South-Africa cohorts (Singhania et al., 2018b) (downloaded from GEO with accession codes GSE107991 and GSE107992, respectively) were imported into R v4.1 for downstream analysis. Raw counts were processed using edgeR v3.36.0 and limma v3.50.0 packages (Robinson et al., 2010; Ritchie et al., 2015). Initial processing of raw counts was performed with edgeR, and genes with counts per million (CPM) lower than 10 in at least 12 samples were discarded from further analysis. Differential expression analysis on the remaining genes was performed using generalized linear models from the limma package. The effect of the sex covariate was taken into account by adding it as a variable to the model. Genes were deemed significant if log₂ fold change was ≥ 1 or ≤ -1 and the false discovery rate (FDR) p -value ≤ 0.05 after Benjamini–Hochberg correction for multiple testing. Plots were obtained using ggplot2 and pheatmap (Wickham, 2016; Kolde, 2019). GSEA was performed on the logFC (aTB vs HD) for Berry London and logFC (aTB vs LTBI) for Berry South Africa, for all genes using ReactomePA (Yu and He, 2016).

Bacteria growth and quantification

M. tuberculosis HN878 and the L4 clinical isolate were expanded in Middlebrook 7H9 (BD Biosciences, Cat. #90003-876) liquid medium supplemented with 10% OADC and 0.2% glycerol (Sigma-Aldrich, Cat. #G5516-500M) and when in mid-log phase bacterial suspensions were aliquoted in cryovials, frozen, and stored at -80°C . Bacterial quantification was performed by thawing six vials of each stock and plating serial dilutions in 7H11 agar medium supplemented with 10% OADC and 0.5% glycerol. The plates were incubated 21 to 28 days at 37°C before colony enumeration.

Animal housing, infection, LXR agonist administration and monitoring

C57BL/6 and C3HeB/FeJ mice were bred and housed at the i3S animal facility. Males and females of 8 to 12 weeks old were used for infections, and maintained under contention conditions in the animal biosafety level 3 facility at i3S, in controlled temperature (20–24°C), humidity (45–65%), and a light cycle of 12h (light/dark). Water and food were provided *ad libitum*. Mice were infected with *M. tuberculosis* (isolate HN878) through the aerosol route using an inhalation exposure system (Glas-Col) (Fonseca et al., 2020; Moreira-Teixeira et al., 2020a; Moreira-Teixeira et al., 2020b). To determine the dose of infection, the bacterial load in the lungs of 3 mice was quantified 3 days post-infection. Doses of infection are indicated in the Figure legends. Infected mice were weighed every week, or every other day when showing signs of disease. Mice were euthanized at the indicated time points or when reaching humane endpoints (weight loss over 20% or poor responsiveness to physical stimulation). For the LXR modulation, mice were treated with 50 µg of LXR agonist T0901317 (Abcam, Cat. #ab142808) or with the vehicle (0,1% DMSO/PBS) administered intraperitoneally, starting on day 7 pre-infection or days 6, 12 or 18 post-infection, every other day until the end of the experiment.

Lung processing

Lungs were aseptically excised and processed as previously described (Fonseca et al., 2020; Moreira-Teixeira et al., 2020a; Moreira-Teixeira et al., 2020b). Briefly, lungs were digested with Collagenase D (Roche, Cat. #11088882001) followed by physical disruption and filtration through 70 µm cell strainers (Falcon, Cat. #352350.0). Cell suspensions were used for colony forming units (CFU) determination, flow cytometry and mRNA analysis.

CFU determination

Lung cell suspensions were lysed with 0.1% saponin, serial dilutions prepared and plated in Middlebrook 7H11 agar (BD Biosciences, Cat. #212203.0) supplemented with OADC and PANTA (BD BioSciences, Cat. # 245114). CFU were enumerated after 21–28 days of incubation at 37°C.

RNA extraction and qPCR

Total RNA was extracted from infected mouse lungs using TRIzol reagent (GRIIP, Cat. #GB23.0100) according to the manufacturer's instructions. cDNA was synthesized with the SuperScript First-Strand Synthesis System for RT-PCR (ThermoScientific, Cat. #E6300L). Target gene mRNA expression was quantified by real-time PCR, using Taqman Primer Probes specific for the target genes, normalized to *Hprt1/Hmbs* (Taqman; Supplementary Table 3).

Flow cytometry

Mouse lung cell suspensions were stained for surface antigens for 30 min at 4° C and fixed for 20 min in 4% paraformaldehyde-PBS after erythrocyte lysis. Dead cells were excluded using ZombieAqua (Biolegend, Cat. #423102). Cells were acquired on a BD Fortessa II and data was analyzed using *FlowJo* software (v10.1.r7). All antibodies used are listed in Supplementary Table 4. Gating strategies are shown in Supplementary Figure 1C.

Histological analysis

Whole lungs were perfused *in situ* with PBS, the right upper lobe was excised, fixed in 10% buffered formalin and embedded in paraffin. Serial 3-µm thick sections were performed and used for hematoxylin and eosin (H&E) staining. Morphometric analysis of the lung pathology was performed as before (Fonseca et al., 2020; Maceiras et al., 2023), with the software Interactive Learning and Segmentation Toolkit (Ilastik version 1.3.3). The probability maps of the whole lung and the lesions were analyzed in CellProfiler Analyst (version 3.1.5). Lesion percentage was defined by the area occupied by lesion in each lung and lesion score by scoring histopathological features (peribronchiolitis, perivascularitis, alveolitis and necrosis/cell debris; Supplementary Figure 1B) as previously reported (Dormans et al., 2004).

Cytokine determination by multiplexed immunoassay

Cytokine levels in the lung supernatants were measured using the LEGENDplex™ Mouse Inflammation Panel kit (Biolegend, Cat. #740446_Mouse Inflammatory Panel) following manufacturer's specifications. The beads were acquired in an BD Accuri C6 (BD Biosciences), and the data analyzed using the LEGENDplex™ Software version 8 (BioLegend).

In vitro cultures and infections

Mouse BMDMs were generated from C57BL/6 bone marrow suspension cells as previously described (Moreira-Teixeira et al., 2016; Fernandes et al., 2025). On day 7 of culture, the macrophages were recovered, plated in 24 well-plates at a density of 1×10^6 cells ml⁻¹ and infected with the indicated *M. tuberculosis* isolates at a multiplicity of infection (MOI) of 2. THP1 cells were grown according to ATCC instructions, differentiated with 100 nM PMA (Sigma-Aldrich, Cat. #16561-29-8) for 24 h, followed by a 48 h rest before infection and then plated in 24 well-plates at a density of 1×10^6 cells ml⁻¹ and infected with *M. tuberculosis* HN878 at a MOI of 1. Where indicated, the LXR agonist T0901317 was added to the cultures at a concentration of 100nM. Bacterial burdens were determined at 4 h and 4 days post-infection by CFU enumeration; and the culture supernatants were collected 24h post-infection for cholesterol analysis. Uninfected cells were used as controls.

Cholesterol quantification

Cholesterol content in the supernatants was measured using the Cholesterol Quantification kit (Sigma-Aldrich, MAK043-1KT) following the manufacturer's instructions. The amount of cholesterol was normalized to that of total protein detected using a BCA protein Assay kit (ThermoFisher, Cat. #23225).

Growth of *M. tuberculosis* in axenic media

M. tuberculosis HN878 was grown in 7H9 supplemented with 10% OADC and 0.05% Tween-80 (Sigma, Cat. #P1754) until mid-exponential phase (OD₆₀₀ of 0.6-0.9). At this stage, a single bacterial suspension was obtained and bacteria were plated in 96-well plates at a final OD of 0.01 in 7H9 medium alone, or with cholesterol and in the presence or absence of the LXR activator T0901317 at a range of concentrations from 0.01 to 10 μM. Cholesterol (Sigma, Cat. #C3045) was dissolved in a solution of tyloxapol and ethanol (Sigma, Cat. #1.00983) (1:1) and added to the medium at a concentration of 200 μM. Cultures were replenished with cholesterol at day 7. Each condition was tested in triplicate. Growth was monitored by measuring the optical density (OD₆₀₀) over the time course of the experiment.

Statistical analysis

Data were analyzed using GraphPad Prism software v8.1.0 or R v4.1. Spearman correlation analysis was performed between the "Radiographic extent of disease" and the SNR and LXR pathways activation, for the Berry - London cohort, to determine the existence of a significant correlation between the two variables. Normality and log normality were assessed using Shapiro-Wilk and outliers with Grubbs test. Statistically significant differences between two groups were determined using non-parametric two-tailed Mann-Whitney U tests. A Log-rank (Mantel-Cox) test was used to analyze the survival curve. Differences were considered significant for $p \leq 0.05$.

Data availability statement

The datasets presented in this study can be found in online repositories. The names of the repository/repository and accession number(s) can be found in the article/[Supplementary Material](#).

Ethics statement

The animal study was approved by i3S Animal Ethics Committee and the Portuguese National Authority for Animal Health (DGAV;

#018413/2021-11-24). The study was conducted in accordance with the local legislation and institutional requirements.

Author contributions

ARM: Investigation, Visualization, Conceptualization, Writing – review & editing, Formal analysis, Data curation, Writing – original draft. MLS: Writing – review & editing, Methodology, Investigation, Writing – original draft, Resources, Visualization, Formal analysis, Conceptualization, Validation. JC: Investigation, Writing – review & editing. RG: Investigation, Writing – review & editing, Writing – original draft. MS: Investigation, Writing – review & editing. SM: Writing – review & editing, Investigation. DM: Writing – review & editing, Investigation. II: Writing – review & editing, Resources, Investigation. AS: Writing – review & editing, Resources, Investigation. CM: Writing – review & editing, Investigation. NN: Writing – review & editing, Investigation, Resources. LS: Resources, Writing – review & editing. PR: Supervision, Writing – review & editing, Funding acquisition. MV: Resources, Writing – original draft, Writing – review & editing. FR: Writing – review & editing, Investigation, Project administration. CW: Supervision, Writing – review & editing. BC: Writing – review & editing, Conceptualization, Investigation, Formal analysis, Project administration, Supervision. MSa: Conceptualization, Supervision, Project administration, Validation, Writing – review & editing, Methodology, Investigation, Formal analysis, Writing – original draft, Funding acquisition, Resources, Visualization.

Funding

The author(s) declare that financial support was received for the research and/or publication of this article. This work was funded by National Funds through FCT—Fundação para a Ciência e a Tecnologia, I.P., under the project UID/4293/2025, and by the La Caixa Foundation, grant HR21-00415 to MS. MLS and RG are funded by FCT PhD scholarships 2020.05061. BD and 2022.12852.BD. FCT also finances GHTM (UID/Multi/04413/2020) and LA-REAL (LA/P/0117/2020). DM is funded by FCT through Estímulo Individual ao Emprego Científico (CEECIND/00241/2017/CP1386/CT0002).

Acknowledgments

We acknowledge the i3S scientific platforms Animal House, Translational Flow Cytometry, Genomics and Histology and Electron Microscopy. We thank Drs Anne O'Garra, Gil Castro, Fabiani Frantz and Tiago Beites for critically reading the manuscript and Dr. Zewen Kelvin Tuong for insightful discussions.

Conflict of interest

The authors declare that the research was conducted in the absence of any commercial or financial relationships that could be construed as a potential conflict of interest.

The author(s) declared that they were an editorial board member of Frontiers, at the time of submission. This had no impact on the peer review process and the final decision.

Generative AI statement

The author(s) declare that no Generative AI was used in the creation of this manuscript.

Any alternative text (alt text) provided alongside figures in this article has been generated by Frontiers with the support of artificial intelligence and reasonable efforts have been made to ensure

References

- Ahsan, F., Maertzdorf, J., Gühlich-Bornhof, U., Kaufmann, S. H. E., and Moura-Alves, P. (2018). IL-36/LXR axis modulates cholesterol metabolism and immune defense to Mycobacterium tuberculosis. *Sci. Rep.* 8, 1520. doi: 10.1038/s41598-018-19476-x
- Berry, M. P., Graham, C. M., McNab, F. W., Xu, Z., Bloch, S. A. A., Oni, T., et al. (2010). An interferon-inducible neutrophil-driven blood transcriptional signature in human tuberculosis. *Nature* 466, 973–977. doi: 10.1038/nature09247
- Bolger, A. M., Lohse, M., and Usadel, B. (2014). Trimmomatic: a flexible trimmer for Illumina sequence data. *Bioinformatics* 30, 2114–2120. doi: 10.1093/bioinformatics/btu170
- Bouttier, M., Laperriere, D., Memari, B., Mangiapane, J., Fiore, A., Mitchell, E., et al. (2016). Alu repeats as transcriptional regulatory platforms in macrophage responses to M. tuberculosis infection. *Nucleic Acids Res.* 44, 10571–10587. doi: 10.1093/nar/gkw782
- Branchett, W. J., Stavropoulos, E., Shields, J., Al-Dibouni, A., Cardoso, M., Fernandes, A. I., et al. (2025). Type I IFN drives neutrophil swarming, impeding lung T cell-macrophage interactions and TB control. *J. Exp. Med.* 222, e20250466. doi: 10.1084/jem.20250466
- Brown, K. L., Wilburn, K. M., Montague, C. R., Grigg, J. C., Sanz, O., Pérez-Herrán, E., et al. (2023). Cyclic AMP-mediated inhibition of cholesterol catabolism in mycobacterium tuberculosis by the novel drug candidate GSK2556286. *Antimicrob. Agents Chemother.* 67, e0129422. doi: 10.1128/aac.01294-22
- Capyk, J. K., D'Angelo, I., Strynadka, N. C., and Eltis, L. D. (2009). Characterization of 3-ketosteroid 9 α -hydroxylase, a Rieske oxygenase in the cholesterol degradation pathway of Mycobacterium tuberculosis. *J. Biol. Chem.* 284, 9937–9946. doi: 10.1074/jbc.M900719200
- Chandra, P., Coullon, H., Agarwal, M., Goss, C. W., and Philips, J. A. (2022). Macrophage global metabolomics identifies cholestenone as host/pathogen cometabolite present in human Mycobacterium tuberculosis infection. *J. Clin. Invest.* 132, e152509. doi: 10.1172/JCI152509
- Chang, J. C., Miner, M. D., Pandey, A. K., Gill, W. P., Harik, N. S., Sasseti, C. M., et al. (2009). igr Genes and Mycobacterium tuberculosis cholesterol metabolism. *J. Bacteriol.* 191, 5232–5239. doi: 10.1128/JB.00452-09
- Chen, Z., Kong, X., Ma, Q., Chen, J., Zeng, Y., Liu, H., et al. (2024). The impact of Mycobacterium tuberculosis on the macrophage cholesterol metabolism pathway. *Front. Immunol.* 15, 1402024. doi: 10.3389/fimmu.2024.1402024
- Coussens, A. K., Zaidi, S. M. A., Allwood, B. W., Dewan, P. K., Gray, G., Kohli, M., et al. (2024). Classification of early tuberculosis states to guide research for improved care and prevention: an international Delphi consensus exercise. *Lancet Respir. Med.* 12, 484–498. doi: 10.1016/S2213-2600(24)00028-6
- Dartois, V. A., Mizrahi, V., Savic, R. M., Silverman, J. A., Hermann, D., and Barry, C. E. III (2025). Strategies for shortening tuberculosis therapy. *Nat. Med.* 31, 1765–1775. doi: 10.1038/s41591-025-03742-3
- Dormans, J., Burger, M., Aguilar, D., Hernandez-Pando, R., Kremer, K., Roholl, P., et al. (2004). Correlation of virulence, lung pathology, bacterial load and delayed type hypersensitivity responses after infection with different Mycobacterium tuberculosis genotypes in a BALB/c mouse model. *Clin. Exp. Immunol.* 137, 460–468. doi: 10.1111/j.1365-2249.2004.02551.x
- Dutta, N. K., Bruiners, N., Zimmerman, M. D., Tan, S., Dartois, V., Gennaro, M. L., et al. (2020). Adjunctive host-directed therapy with statins improves tuberculosis-related outcomes in mice. *J. Infect. Dis.* 221, 1079–1087. doi: 10.1093/infdis/jiz517
- El Kasmi, K. C., Qualls, J. E., Pesce, J. T., Smith, A. M., Thompson, R. W., Henaotamayo, M., et al. (2008). Toll-like receptor-induced arginase 1 in macrophages thwarts effective immunity against intracellular pathogens. *Nat. Immunol.* 9, 1399–1406. doi: 10.1038/ni.1671
- Fernandes, A. I., Pinto, A. J., Silvério, D., Zedler, U., Ferreira, C., Duarte, I. F., et al. (2025). Genetically diverse mycobacterium tuberculosis isolates manipulate inflammasomes and interleukin 1 β secretion independently of macrophage metabolic rewiring. *J. Infect. Dis.* 231, e671–e684. doi: 10.1093/infdis/jiae583
- Fonseca, K. L., Maceiras, A. R., Matos, R., Simoes-Costa, L., Sousa, J., Cá, B., et al. (2020). Deficiency in the glycosyltransferase Gnt1 increases susceptibility to tuberculosis through a mechanism involving neutrophils. *Mucosal Immunol.* 13, 836–848. doi: 10.1038/s41385-020-0277-7
- Foo, C. X., Bartlett, S., and Ronacher, K. (2022). Oxysterols in the immune response to bacterial and viral infections. *Cells* 11, 201. doi: 10.3390/cells11020201
- Garton, N. J., Waddell, S. J., Sherratt, A. L., Lee, S.-M., Smith, R. J., Senner, C., et al. (2008). Cytological and transcript analyses reveal fat and lazy persister-like bacilli in tuberculous sputum. *PLoS Med.* 5, e75. doi: 10.1371/journal.pmed.0050075
- Gern, B. H., Klas, J. M., Foster, K. A., Kanagy, M. E., Cohen, S. B., Plumlee, C. R., et al. (2025). Early and opposing neutrophil and CD4 T cell responses shape pulmonary tuberculosis pathology. *J. Exp. Med.* 222, e20250161. doi: 10.1084/jem.20250161
- Glaria, E., Letelier, N. A., and Valledor, A. F. (2020). Integrating the roles of liver X receptors in inflammation and infection: mechanisms and outcomes. *Curr. Opin. Pharmacol.* 53, 55–65. doi: 10.1016/j.coph.2020.05.001
- Gleeson, L. E., Sheedy, F. J., Palsson-McDermott, E. M., Triglia, D., O Leary, S. M., O Sullivan, M. P., et al. (2016). Cutting edge: mycobacterium tuberculosis induces aerobic glycolysis in human alveolar macrophages that is required for control of intracellular bacillary replication. *J. Immunol.* 196, 2444–2449. doi: 10.4049/jimmunol.1501612
- Han, M., Liang, L., Liu, L., Yue, J., Zhao, Y., and Xiao, H. (2014). Liver X receptor gene polymorphisms in tuberculosis: effect on susceptibility. *PLoS One* 9, e95954. doi: 10.1371/journal.pone.0095954
- Hu, Y., Van Der Geize, R., Besra, G. S., Gurcha, S. S., Liu, A., Rohde, M., et al. (2010). 3-Ketosteroid 9 α -hydroxylase is an essential factor in the pathogenesis of Mycobacterium tuberculosis. *Mol. Microbiol.* 75, 107–121. doi: 10.1111/j.1365-2958.2009.06957.x
- Huang, L., Nazarova, E. V., Tan, S., Liu, Y., and Russell, D. G. (2018). Growth of Mycobacterium tuberculosis *in vivo* segregates with host macrophage metabolism and ontogeny. *J. Exp. Med.* 215, 1135–1152. doi: 10.1084/jem.20172020
- Joseph, S. B., Bradley, M. N., Castrillo, A., Bruhn, K. W., Mak, P. A., Pei, L., et al. (2004). LXR-dependent gene expression is important for macrophage survival and the innate immune response. *Cell* 119, 299–309. doi: 10.1016/j.cell.2004.09.032
- Kathayat, D., and VanderVen, B. C. (2024). Exploiting cAMP signaling in Mycobacterium tuberculosis for drug discovery. *Trends Microbiol.* 32, 874–883. doi: 10.1016/j.tim.2024.01.008

accuracy, including review by the authors wherever possible. If you identify any issues, please contact us.

Publisher's note

All claims expressed in this article are solely those of the authors and do not necessarily represent those of their affiliated organizations, or those of the publisher, the editors and the reviewers. Any product that may be evaluated in this article, or claim that may be made by its manufacturer, is not guaranteed or endorsed by the publisher.

Supplementary material

The Supplementary Material for this article can be found online at: <https://www.frontiersin.org/articles/10.3389/fcimb.2025.1724798/full#supplementary-material>

- Kim, M. J., Wainwright, H. C., Lockett, M., Bekker, L.-G., and Walther, G. B. (2010). Cessation of human tuberculosis granulomas correlates with elevated host lipid metabolism. *EMBO Mol. Med.* 2, 258–274. doi: 10.1002/emmm.201000079
- Kim, D., Paggi, J. M., Park, C., Bennett, C., and Salzberg, S. L. (2019). Graph-based genome alignment and genotyping with HISAT2 and HISAT-genotype. *Nat. Biotechnol.* 37, 907–915. doi: 10.1038/s41587-019-0201-4
- Kolde, R. (2019). *Pheatmap: Pretty heatmaps*.
- Korf, H., Beken, S. V., Romano, M., Steffensen, K. R., Stijlemans, B., Gustafsson, J. Å., et al. (2009). Liver X receptors contribute to the protective immune response against *Mycobacterium tuberculosis* in mice. *J. Clin. Invest.* 119, 1626–1637. doi: 10.1172/JCI35288
- Kumar, R., Singh, P., Kolloli, A., Shi, L., Bushkin, Y., Tyagi, S., et al. (2019). Immunometabolism of phagocytes during *Mycobacterium tuberculosis* infection. *Front. Mol. Biosci.* 6, 105. doi: 10.3389/fmolb.2019.00105
- Lachmandas, E., Beigier-Bompadre, M., Cheng, S. C., Kumar, V., van Laarhoven, A., Wang, X., et al. (2016). Rewiring cellular metabolism via the AKT/mTOR pathway contributes to host defence against *Mycobacterium tuberculosis* in human and murine cells. *Eur. J. Immunol.* 46, 2574–2586. doi: 10.1002/eji.201546259
- Lai, R. P. J., Cortes, T., Marais, S., Rockwood, N., Burke, M. L., Garza-Garcia, A., et al. (2021). Transcriptomic characterization of tuberculosis sputum reveals a host warburg effect and microbial cholesterol catabolism. *mBio* 12, e0176621. doi: 10.1128/mBio.01766-21
- Leopold Wager, C. M., Arnett, E., and Schlesinger, L. S. (2019a). Macrophage nuclear receptors: Emerging key players in infectious diseases. *PLoS Pathog.* 15, e1007585. doi: 10.1371/journal.ppat.1007585
- Leopold Wager, C. M., Arnett, E., and Schlesinger, L. S. (2019b). *Mycobacterium tuberculosis* and macrophage nuclear receptors: What we do and don't know. *Tuberculosis (Edinb)* 116S, S98–S106. doi: 10.1016/j.tube.2019.04.016
- Luo, J., Yang, H., and Song, B. L. (2020). Mechanisms and regulation of cholesterol homeostasis. *Nat. Rev. Mol. Cell Biol.* 21, 225–245. doi: 10.1038/s41580-019-0190-7
- Maceiras, A. R., Silverio, D., Goncalves, R., Cardoso, M. S., and Saraiva, M. (2023). Infection with hypervirulent *Mycobacterium tuberculosis* triggers emergency myelopoiesis but not trained immunity. *Front. Immunol.* 14, 1211404. doi: 10.3389/fimmu.2023.1211404
- Mahajan, S., Dkhar, H. K., Chandra, V., Dave, S., Nanduri, R., Janmeja, A. K., et al. (2012). *Mycobacterium tuberculosis* modulates macrophage lipid-sensing nuclear receptors PPARgamma and TR4 for survival. *J. Immunol.* 188, 5593–5603. doi: 10.4049/jimmunol.1103038
- Matalonga, J., Glaria, E., Bresque, M., Escandé, C., Carbó, J. M., Kiefer, K., et al. (2017). The nuclear receptor LXR limits bacterial infection of host macrophages through a mechanism that impacts cellular NAD metabolism. *Cell Rep.* 18, 1241–1255. doi: 10.1016/j.celrep.2017.01.007
- Mendonca, L. E., Pernet, E., Khan, N., Sanz, J., Kaufmann, E., Downey, J., et al. (2022). Human alveolar macrophage metabolism is compromised during *Mycobacterium tuberculosis* infection. *Front. Immunol.* 13, 1044592. doi: 10.3389/fimmu.2022.1044592
- Moopanar, K., Nomfundo, A., Nyide, G., Senzani, S., and Mvub, N. E. (2023). Clinical strains of *Mycobacterium tuberculosis* exhibit differential lipid metabolism-associated transcriptome changes in *in vitro* cholesterol and infection models. *Pathog. Dis.* 81, ftac046. doi: 10.1093/femspd/ftac046
- Moreira-Teixeira, L., Sousa, J., McNab, F. W., Torrado, E., Cardoso, F., Machado, H., et al. (2016). Type I IFN Inhibits Alternative Macrophage Activation during *Mycobacterium tuberculosis* Infection and Leads to Enhanced Protection in the Absence of IFN-gamma Signaling. *J. Immunol.* 197, 4714–4726. doi: 10.4049/jimmunol.1600584
- Moreira-Teixeira, L., Tabone, O., Graham, C. M., Singhania, A., Stavropoulos, E., Redford, P. S., et al. (2020a). Mouse transcriptome reveals potential signatures of protection and pathogenesis in human tuberculosis. *Nat. Immunol.* 21, 464–476. doi: 10.1038/s41590-020-0610-z
- Moreira-Teixeira, L., Stimpson, P. J., Stavropoulos, E., Hadebe, S., Chakravarty, P., Ioannou, M., et al. (2020b). Type I IFN exacerbates disease in tuberculosis-susceptible mice by inducing neutrophil-mediated lung inflammation and NETosis. *Nat. Commun.* 11, 5566. doi: 10.1038/s41467-020-19412-6
- Nesbitt, N. M., Yang, X., Fontan, P., Kolesnikova, I., Smith, L., Sampson, N. S., et al. (2010). A thiolase of *Mycobacterium tuberculosis* is required for virulence and production of androstenedione and androstadienedione from cholesterol. *Infect. Immun.* 78, 275–282. doi: 10.1128/IAI.00893-09
- Ngo, M. D., Bartlett, S., Bielefeldt-Ohmann, H., Foo, C. X., Sinha, R., Arachchige, B. J., et al. (2022). A blunted GPR183/oxysterol axis during dysglycemia results in delayed recruitment of macrophages to the lung during *Mycobacterium tuberculosis* infection. *J. Infect. Dis.* 225, 2219–2228. doi: 10.1093/infdis/jiac102
- O'Garra, A., Redford, P. S., McNab, F. W., Bloom, C. I., Wilkinson, R. J., Berry, M. P. R., et al. (2013). The immune response in tuberculosis. *Annu. Rev. Immunol.* 31, 475–527. doi: 10.1146/annurev-immunol-032712-095939
- Organization, W.H. (2024). *Global tuberculosis report 2024* (Geneva: World Health Organization).
- Ouellet, H., Guan, S., Johnston, J. B., Chow, E. D., Kells, P. M., Burlingame, A. L., et al. (2010). *Mycobacterium tuberculosis* CYP125A1, a steroid C27 monooxygenase that detoxifies intracellularly generated cholest-4-en-3-one. *Mol. Microbiol.* 77, 730–742. doi: 10.1111/j.1365-2958.2010.07243.x
- Pandey, A. K., and Sasseti, C. M. (2008). *Mycobacterial persistence* requires the utilization of host cholesterol. *Proc. Natl. Acad. Sci. U.S.A.* 105, 4376–4380. doi: 10.1073/pnas.0711159105
- Parihar, S. P., Guler, R., Khutlang, R., Lang, D. M., Hurdal, R., Mhlanga, M. M., et al. (2014). Statin therapy reduces the *Mycobacterium tuberculosis* burden in human macrophages and in mice by enhancing autophagy and phagosome maturation. *J. Infect. Dis.* 209, 754–763. doi: 10.1093/infdis/jit550
- Pertea, M., Pertea, G. M., Antonescu, C. M., Chang, T. C., Mendell, J. T., and Salzberg, S. L. (2015). StringTie enables improved reconstruction of a transcriptome from RNA-seq reads. *Nat. Biotechnol.* 33, 290–295. doi: 10.1038/nbt.3122
- Pisu, D., Huang, L., Grenier, J. K., and Russell, D. G. (2020). Dual RNA-seq of mtb-infected macrophages *in vivo* reveals ontologically distinct host-pathogen interactions. *Cell Rep.* 30, 335–350 e4. doi: 10.1016/j.celrep.2019.12.033
- Pisu, D., Huang, L., Narang, V., Theriault, M., Lé-Bury, G., Lee, B., et al. (2021). Single cell analysis of *M. tuberculosis* phenotype and macrophage lineages in the infected lung. *J. Exp. Med.* 218, 335–350.e4. doi: 10.1084/jem.20210615
- Ritchie, M. E., Phipson, B., Wu, D., Hu, Y., Law, C. W., Shi, W., et al. (2015). limma powers differential expression analyses for RNA-sequencing and microarray studies. *Nucleic Acids Res.* 43, e47. doi: 10.1093/nar/gkv007
- Robinson, M. D., McCarthy, D. J., and Smyth, G. K. (2010). edgeR: a Bioconductor package for differential expression analysis of digital gene expression data. *Bioinformatics* 26, 139–140. doi: 10.1093/bioinformatics/btp616
- Roth, A. T., Philips, J. A., and Chandra, P. (2024). The role of cholesterol and its oxidation products in tuberculosis pathogenesis. *Immunometabolism (Cobham)* 6, e00042. doi: 10.1097/IN9.000000000000042
- Russell, D. G., Simwela, N. V., Mattila, J. T., Flynn, J., Mwandumba, H. C., and Pisu, D. (2025). How macrophage heterogeneity affects tuberculosis disease and therapy. *Nat. Rev. Immunol.* 25, 370–384. doi: 10.1038/s41577-024-01124-3
- Scriba, T. J., Maseeme, M., Young, C., Taylor, L., and Leslie, A. J. (2024). Immunopathology in human tuberculosis. *Sci. Immunol.* 9, eado5951. doi: 10.1126/sciimmunol.ado5951
- Sever, R., and Glass, C. K. (2013). Signaling by nuclear receptors. *Cold Spring Harb. Perspect. Biol.* 5, a016709. doi: 10.1101/cshperspect.a016709
- Shi, L., Salamon, H., Eugenin, E. A., Pine, R., Cooper, A., and Gennaro, M. L. (2015). Infection with *Mycobacterium tuberculosis* induces the Warburg effect in mouse lungs. *Sci. Rep.* 5, 18176. doi: 10.1038/srep18176
- Singhania, A., Wilkinson, R. J., Rodrigue, M., and Haldar, P. (2018a). The value of transcriptomics in advancing knowledge of the immune response and diagnosis in tuberculosis. *Nat. Immunol.* 19, 1159–1168. doi: 10.1038/s41590-018-0225-9
- Singhania, A., et al. (2018b). A modular transcriptional signature identifies phenotypic heterogeneity of human tuberculosis infection. *Nat. Commun.* 9, 2308. doi: 10.1038/s41467-018-04579-w
- Soto-Ramirez, M. D., et al. (2017). Cholesterol plays a larger role during *Mycobacterium tuberculosis in vitro* dormancy and reactivation than previously suspected. *Tuberculosis (Edinb)* 103, 1–9. doi: 10.1016/j.tube.2016.12.004
- Tabone, O., et al. (2021). Blood transcriptomics reveal the evolution and resolution of the immune response in tuberculosis. *J. Exp. Med.* 218, e20210915. doi: 10.1084/jem.20210915
- Valledor, A. F., et al. (2004). Activation of liver X receptors and retinoid X receptors prevents bacterial-induced macrophage apoptosis. *Proc. Natl. Acad. Sci. U.S.A.* 101, 17813–17818. doi: 10.1073/pnas.0407749101
- VanderVen, B. C., et al. (2015). Novel inhibitors of cholesterol degradation in *Mycobacterium tuberculosis* reveal how the bacterium's metabolism is constrained by the intracellular environment. *PLoS Pathog.* 11, e1004679. doi: 10.1371/journal.ppat.1004679
- Varakka, T., et al. (2021). Metabolic fate of human immunoreactive sterols in *Mycobacterium tuberculosis*. *J. Mol. Biol.* 433, 166763. doi: 10.1016/j.jmb.2020.166763
- Wheelwright, M., et al. (2014). All-trans retinoic acid-triggered antimicrobial activity against *Mycobacterium tuberculosis* is dependent on NPC2. *J. Immunol.* 192, 2280–2290. doi: 10.4049/jimmunol.1301686
- Wickham, H. (2016). *ggplot2: Elegant Graphics for Data Analysis*. RStudio, Houston, USA.
- Wilburn, K. M., et al. (2022). Pharmacological and genetic activation of cAMP synthesis disrupts cholesterol utilization in *Mycobacterium tuberculosis*. *PLoS Pathog.* 18, e1009862. doi: 10.1371/journal.ppat.1009862
- Wilburn, K. M., Fieweger, R. A., and VanderVen, B. C. (2018). Cholesterol and fatty acids grease the wheels of *Mycobacterium tuberculosis* pathogenesis. *Pathog. Dis.* 76, fty021. doi: 10.1093/femspd/fty021
- Yam, K. C., et al. (2009). Studies of a ring-cleaving dioxygenase illuminate the role of cholesterol metabolism in the pathogenesis of *Mycobacterium tuberculosis*. *PLoS Pathog.* 5, e1000344. doi: 10.1371/journal.ppat.1000344
- Yu, G., and He, Q. Y. (2016). ReactomePA: an R/Bioconductor package for reactome pathway analysis and visualization. *Mol. Biosyst.* 12, 477–479. doi: 10.1039/C5MB00663E